ELSEVIER

International Journal of Mass Spectrometry 207 (2001) 145–152

International Journal of Mass Spectrometry

High-resolution analysis of the kinetic energy distribution of fragment ions produced by dissociative ionization of propane

T. Fiegele[a], C. Mair[a], P. Scheier[a], K. Becker[b], T.D. Märk[a,c,*]

[a]*Institut für Ionenphysik, Leopold-Franzens Universität, Innsbruck, Austria*
[b]*Department of Physics and Engineering Physics, Stevens Institute of Technology, Hoboken, NJ 07030, USA*
[c]*Department of Plasma Physics, Comenius University, Mlynska dolina, SK-84248 Bratislava, Slovakia*

Received 5 October 2000; accepted 14 December 2000

Abstract

We report measurements of the kinetic energy distributions of fragment ions produced by electron impact dissociative ionization of propane using a two-sector-field mass spectrometer in conjunction with the retarding field method. This technique achieves a higher energy resolution, albeit at much reduced ion signals and at a significant loss of energetic fragment ions compared to the conventional ion deflection technique, which has been used extensively by other groups in the past. The higher energy resolution used in the present experiments results in a complete separation of the thermal/quasi-thermal fragment ions from the energetic fragment ions. This, in turn, reveals that the energetic fragment ions have a much narrower kinetic energy distribution than previously assumed. Because of the comparatively weak ion signals, further studies such as separate threshold cross-section measurements and appearance energy determinations for, respectively, the "slow" and "fast" fragment ions could only be carried out for the CH_3^+ and $C_2H_4^+$ fragment ions. (Int J Mass Spectrom 207 (2001) 145–152) © 2001 Elsevier Science B.V.

Keywords: Electron-impact ionization; Kinetic energy distributions; Hydrocarbons

1. Introduction

The dissociative ionization of a molecule induced by electron impact is a very important process in low-temperature plasmas, excimer lasers, radiation chemistry, edge plasmas in fusion reactors, mass spectrometry, and chemical analysis [1–8]. Fragment ions produced via dissociative ionization often carry substantial amounts of kinetic energy, and the kinetic energy distribution of a particular fragment ion determines the energy deposition and the energy transfer pathways in the corresponding media. Thus, the modeling of environments where dissociative ionization processes are important requires knowledge not only of the production efficiency and the nature of fragment ions produced but also of their kinetic energy distribution. Hydrocarbons, which are abundant constituents of planetary atmospheres and major compounds in combustible gas mixtures and in fusion edge plasmas [1–8], are known to form fragment ions with broad kinetic energy distributions ranging from thermal energies to many electronvolts. In some cases, such as, for instance, propane, many of the energetic ions are formed with higher probabilities than the thermal ions (see, e.g., Poll et al. [9] and references cited therein).

*Corresponding author. E-mail: tilmann.maerk@uibk.ac.at

PII S1387-3806(01)00364-5

Propane, C_3H_8, is a prototypical hydrocarbon molecule whose absolute total and partial photon [10] and electron [11–13] ionization cross sections and nascent fragment ion energy distributions [9,13–22] have been studied extensively. In addition, a number of experimental [23–30] and theoretical studies [31] exist on the details of fragment ion formation. All previous studies [9,14–22] found that essentially all fragment ions of propane are formed with complex energy distributions with two major components, a low-energy component comprised of thermal and/or quasi-thermal ("slow") ions with maximum kinetic energies of $\lesssim$0.3 eV and energetic ("fast") ions with a broad energy distribution from 0.5 eV to $\sim$5 eV. It has been suggested that several dissociation pathways contribute to the formation of the various fragment ions, as demonstrated by the different appearance energies that were measured for the respective slow and fast component in the kinetic energy distribution of a given fragment ion [14,32].

Most experimental studies of the kinetic energy release distributions (KERDs) of fragment ions produced by electron impact on propane described in the literature to date used the well-known deflection method [9,13–22]. The ions formed in the ion source by dissociative ionization are extracted and deflected across the entrance aperture of a mass-selective device, for example, a mass spectrometer. For a given fragment ion, the ion signal is recorded as a function of the deflection voltage, and the distribution that is obtained can be converted into a kinetic energy distribution. The advantage of this technique is the complete transmission of all ions, including the most energetic ions, from the ion source through the mass spectrometer without discrimination (see, e.g., [9,13,22]). The disadvantages include the fact that the absolute calibration of the energy scale is difficult and often has to rely on previously measured data (see [17]), a comparatively poor energy resolution, and the fact that the measurement is indirect in the sense that the data analysis involves taking the derivative of the recorded ion distribution.

As described in detail by Franklin and coworkers [20], some of the earlier investigations either used retarding field methods [33–37] or analyzed peak shapes using sector-field and time-of-flight instruments (see also a number of recent very successful applications of this later method [38–43] including PIFCO [44], PEPICO [45–48], and TPEPICO [49–51] techniques to prepare energy-selected parent ions for the TOF analysis, yielding detailed information about the energetics and dynamics of the decay reaction). As an alternative, the energy distribution of the fragment ions can also be determined using a retarding field method. (It is interesting to note that as another alternative Doppler broadening [52,53] has been used, but this method requires high-resolution spectroscopic techniques.) This technique, employed in some very early papers [33–37], uses the mass-dispersive element (mass spectrometer) to select a particular fragment ion, and (limited) information about the kinetic energy of fragment ions has been obtained by using a retarding field either before the mass spectrometer (employing the metastable suppressor as retarding element) [37] or in front of the ion detector [35].

In this article, we report measurements of the kinetic energy distributions of fragment ions produced by electron-impact dissociative ionization of propane using a retarding field detector after the ions have passed a double-focusing two-sector field mass spectrometer. The advantages of this method compared to the deflection method are a much higher energy resolution (see below: the comparison of KERDs measured with both methods indicating an order of magnitude difference in the energy resolution) and the fact that the energy distribution is obtained directly after differentiation of the measured, integrated distribution curve. The advantage of this method compared to the earlier retarding field methods is the possibility to record full kinetic energy distributions of the fragment ions with no interference from the mass-dispersive element caused by the double-focusing action of the mass analyzer used. The disadvantage of this method compared to the deflection method is that only a small fraction of the energetic fragment ions extracted from the ion source are passing the mass spectrometer. As no sweep of the entire ion distribution across the entrance slit of the mass spectrometer is carried out, only those fragment ions

that move in the direction of the mass spectrometer are collected. This results in a substantial discrimination effect (see the calculations carried out in [13,22]) and in a significant reduction in the recorded ion signal for energetic ions. Nevertheless, the higher energy resolution (judging from similar measurements about the energy resolution in ion/surface collision experiments, the resolution to be achieved by this method lies in the tens of meV range [54,55]) results in a complete separation of the thermal and quasi-thermal fragment ions from the energetic ions, which in turn, reveals that the energetic fragment ions have a much narrower kinetic energy distribution than previously assumed. Because of the comparatively weak ion signals, further studies such as separate threshold cross-section measurements and appearance energy determinations for slow and fast fragment ions could only be carried out for the CH_3^+ and $C_2H_4^+$ fragment ions.

2. Experimental details

A detailed description of the apparatus used in the present studies has already been given in several earlier publications to which we refer the reader for further details [9,13,22,54]. Briefly, we use a double-focusing Nier-Johnson two-sector-field mass spectrometer of reversed geometry with a Nier-type electron-impact ion source. The target gas beam is crossed by a well-characterized magnetically collimated electron beam with a FWHM energy spread of ~0.5 eV. The product ions are extracted from the ion source by a penetrating electric field, accelerated to ~3 kV, and enter the mass spectrometer through a narrow entrance slit after passing a pair of mutually perpendicular deflection plates. In the present mode of operation, the deflection plates are not used to sweep the ion beam across the mass spectrometer entrance slit but are kept at fixed voltages and are only used for minor corrections of the ion trajectories to maximize the ion flux into the mass spectrometer. After passing through a magnetic sector field for momentum analysis, the ions enter a field-free region followed by an electric sector field, which acts as an energy analyzer.

The combined action of the two fields in a double-focusing mass spectrometer results in a mass-selected ion beam leaving the mass spectrometer that contains all ions of a given mass-to-charge ratio irrespective of their initial kinetic energy within certain limits, that is, depending on the width of the β-slit that is located between the two sector fields of the mass spectrometer. This mass-selected ion beam, which contains all the information with respect to the ion energy distribution before mass analysis, is then analyzed using a retarding field method developed recently in our laboratory in the course of ion–surface interaction experiments [54]. In these experiments, the energy spread of the primary ion beam was determined by applying a retarding potential to the surface and measuring the (reflected) total ion signal as a function of the surface potential. If one assumes that there is no or only negligible interference between the electric fields in the detector region and the retarding field, the energy spread (kinetic energy distribution) is obtained as the first derivative of the total ion signal. Further details of this method are given in [54,55].

3. Results and discussion

Figs. 1 and 2 show two sets of kinetic energy distributions obtained with the present apparatus. Fig. 1 shows the distributions obtained for the CH_i^+ (i = 1–3) fragment ions along with the distribution of the parent $C_3H_8^+$ ion, while Fig. 2, shows the measured distributions for the $C_2H_i^+$ (i = 3–5) fragment ions (again together with the parent ion distribution). The width of the parent ion distribution is caused by the thermal width, which is caused by the temperature of the ion source (~500 K), and by the width, which is caused by the inherent limitation in instrumental resolution caused by the electron impact ionization process itself as well as by the ion extraction procedure. In our case, the overall nominal energy resolution (defined here as the FWHM of the thermal peak of the parent ion) was ~0.085 eV [55] in good agreement with earlier determinations [54]. We note that the spectra in Figs. 1 and 2 show the recorded data without any correction for ion discrimination

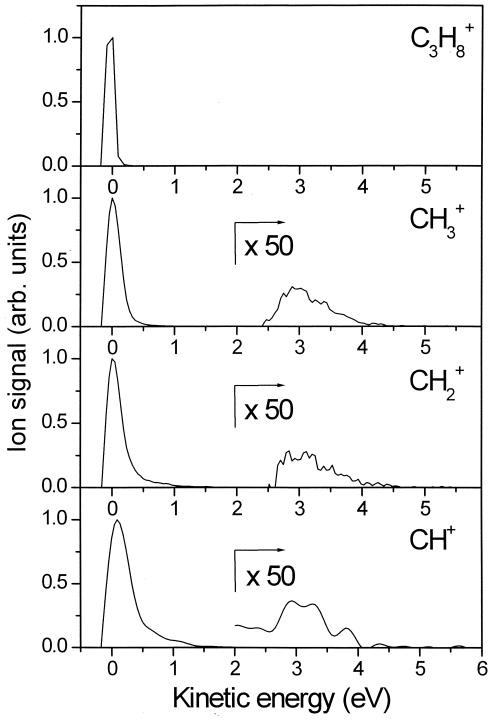

Fig. 1. Kinetic energy distribution of CH_i^+ (i=1–3) fragment ions following dissociative electron impact ionization of C_3H_8 by 100 eV electrons. Also shown for reason of comparison is the distribution for the $C_3H_8^+$ parent ions.

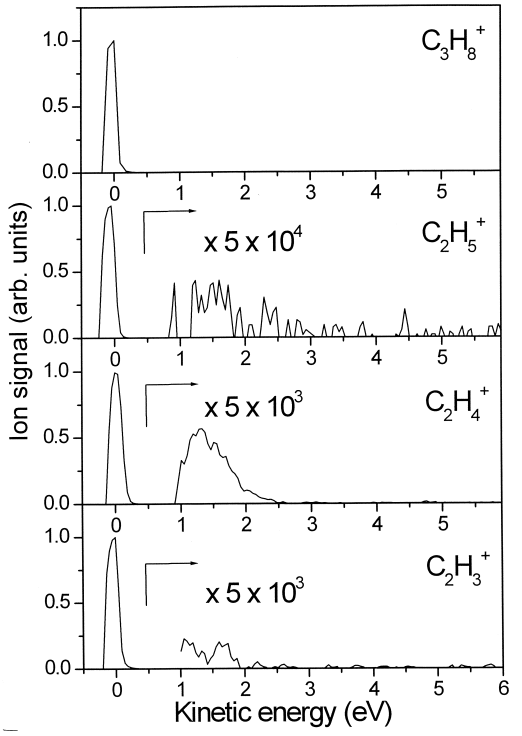

Fig. 2. Kinetic energy distribution of $C_2H_i^+$ (i=3–5) fragment ions following dissociative electron impact ionization of C_3H_8 by 100 eV electrons. Also shown for reason of comparison is the distribution for the $C_3H_8^+$ parent ions.

effects (see the detailed discussion in [9] demonstrating the necessity for large corrections for the higher-energy fragment ions to arrive at true relative detection efficiencies). The same holds true for all other spectra presented in this article.

The spectra shown in Figs. 1 and 2 clearly depict the advantage and disadvantage of the retarding field method for these studies. On one hand, the spectra show the thermal/quasi-thermal (slow) component and the energetic (fast) component in the kinetic energy spectrum clearly resolved. On the other hand, the ion signals obtained for the fast components are very weak. These two facts become even more apparent from the spectra for the CH_3^+ fragment ion shown in Fig. 3, where we compare the present data with several previously reported kinetic energy distributions that were all obtained from measurements using the deflection technique.

We further note that the slow distribution in the various fragment ion spectra is always broader than the $C_3H_8^+$ parent ion distribution and that the width of the slow component becomes increasingly broader and the maximum in the distribution is shifted to higher energies as one goes to lighter and lighter fragment ions. This is to be expected for fragmentation induced by vibrational predissociation involving a certain kinetic energy release and has been discussed in detail in [9]. Thus, the slow component in the ion spectra is often referred to as the "thermal/quasi-thermal" or simply the "quasi-thermal" component rather than the "thermal" component.

Perhaps the most striking observation from our measured spectra is the fact that the quasi-thermal and the energetic fragment ions are completely separated. No fragment ions (within the present detection limit) are formed with kinetic energies in the range of 0.8–2.5 eV in the case of CH_i^+ (i = 1–3) or between

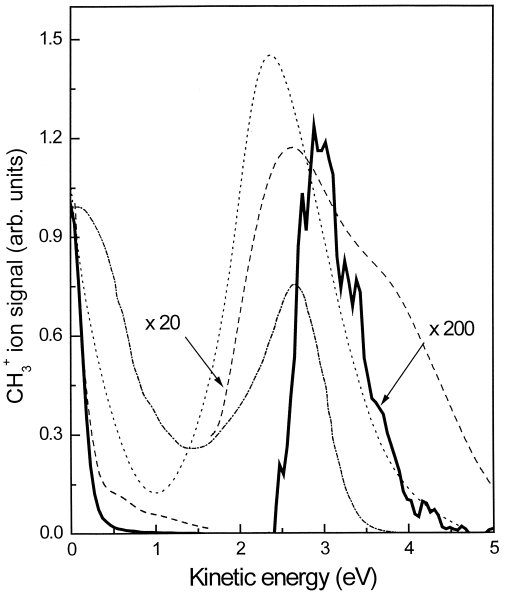

Fig. 3. Kinetic energy distributions of CH_3^+ fragment ions following dissociative electron impact ionization of C_3H_8. The various curves represent the present data (thick solid line) in comparison with the data of Poll et al. [9] (long dashed line), Fuchs and Taubert [16] (short dashed line), and Ehrhardt and Tekaat [14] (dash-dot line).

0.3 and 1 eV in the case of $C_2H_i^+$ (i = 3–5). Furthermore, there are well-defined high-energy cut-off energies in both cases, ~4 eV for CH_i^+ and ~2 eV for $C_2H_i^+$, above which no fragment ions appear in our measured spectra at all. These findings are different from all previously reported measurements, which showed more or less continuous energy distributions (with some structure) from zero energy to 5 eV (CH_i^+) or 3 eV ($C_2H_i^+$). Thus, our measurements indicate that the range of kinetic energies of these fragment ions is much more restricted than previously assumed.

The following additional observations are noteworthy. First, the peak value for the high-energy distributions measured for the CH_i^+ (i = 1–3) fragment ions is at roughly the same energy for all three ions, namely at ~2.9 eV with an uncertainty of ~0.3 eV because of the low signal (as compared to the thermal peak; this relatively low signal is, however, mainly because of discrimination; see [9]) and, thus, large scatter for these high-energy curves. Note that the optimum true energy resolution is much better (in the several tens of meV region), allowing us to obtain quite accurate values for the FWHM values of the quasi-thermal peaks (see below; Fig. 4).

Second, the peak in the distributions measured for the $C_2H_i^+$ (i = 3–5) fragment ions is also at roughly the same energy for all three ions, namely, at ~1.5 eV (even though the determination of the peak in these spectra is more difficult, because of the lower signals, and the peak value carries a larger margin of error).

Third, in the case of CH_3^+, the difference in the

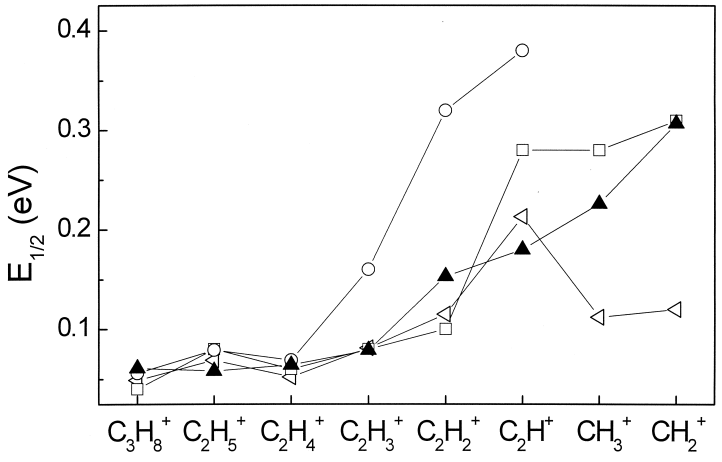

Fig. 4. Measured FWHM width, $E_{1/2}$, of the measured kinetic energy distribution for various fragment ions. The four data sets refer to the present data (filled triangles), the data from Poll et al. [9] (open inverted triangles), Grill et al. [13] (open squares), and Taubert [17] (open circles).

kinetic energy values that correspond to the peaks in, respectively, the quasi-thermal distribution and the fast distribution is ~2.8 eV, which is in good agreement with previously reported values that range from 2.2 to 2.9 eV [17,19,56–58].

A possible analysis of the formation of the quasi-thermal fragment ions is summarized in Fig. 4. In this figure, we display the measured FWHM values of the kinetic energy distributions ($E_{1/2}$) of various quasi-thermal fragment ions in comparison with results from previous measurements [9,13,17]. We find a gradual increase of the values of $E_{1/2}$ from ~50 to 300 meV as we go to lighter fragment ions. The present data are in good to satisfactory agreement with previous data obtained in this laboratory using the deflection method [9,13], but they do not reproduce the rather steep increase that was reported by Taubert [17] for the lighter fragment ions.

Additional measurements such as separate threshold cross-section measurements for individual ion distributions (i.e., concerning ions from the slow and fast components, respectively) and appearance energy determinations as shown in Fig. 5 were carried out only for the two most intense fragment ions, CH_3^+ and $C_2H_4^+$. The two solid lines in Fig. 5 represent the appearance energies of, respectively, the Ar^+ and Ar^{2+} ions that served as calibration points of the electron energy scale. For each ion, appearance energy measurements were carried out separately for, respectively, the quasi-thermal and the fast fragment ions. The quasi-thermal components show the expected low appearance energies at ~12 eV ($C_2H_4^+$) and 15 eV (CH_3^+). The value of 12 eV (where no structure at all is evident in the low-energy region of the respective ion yield) is in excellent agreement with recent high-resolution electron-impact results (using a crossed-beam apparatus including a hemispherical electron monochromator) by Fiegele et al. [59] and tabulated literature values; for example, for the appearance energy of $C_2H_4^+$, Fiegele et al. [59] reported a value of 11.94 ± 0.1 eV. The corresponding values obtained in the earlier measurements by Erhardt and Tekaat [14] using the deflection method are 11.4 and 15.2 eV, respectively. In the case of CH_3^+, the most likely formation process for the ions

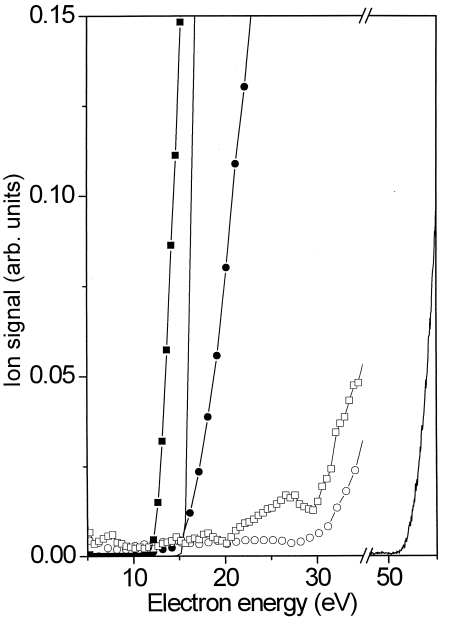

Fig. 5. Recorded ion signals as a function of energy of the ionizing electrons. The two solid lines represent the appearance-energy curves for, respectively, Ar^+ and Ar^{2+}, which served to calibrate the energy scale. The various symbols refer to the quasi-thermal CH_3^+ ions (filled circles), the "fast" CH_3^+ ions (open circles), the quasi-thermal $C_2H_4^+$ ions (filled squares), and the "fast" $C_2H_4^+$ ions (open squares).

appearing at ~15 eV is, according to [14], the break-up of the initially formed $C_3H_8^+$ ion:

$$C_3H_8^+ \rightarrow CH_3^+ + H_2 + C_2H_3 \quad (1)$$

with a thermochemical minimum energy of 15.15 eV [14]. Nonetheless, as the C_2H_5 radical is bound with respect to $C_2H_3+H_2$, there should be CH_3^+ ions below the above-mentioned thermochemical threshold, and indeed, the present data show structure in the low-energy region, which suggests that an additional process contributes to the formation of these ions below the 15-eV threshold in accordance with an appearance energy for this process at 14.0±0.5 eV [60,61]. In the case of $C_2H_4^+$, the most likely process is

$$C_3H_8^+ \rightarrow C_2H_4^+ + CH_4 \quad (2)$$

with a thermochemical minimum energy of 11.36 eV [14].

As expected, the appearance energy measurements for the fast fragment ion component reveal significantly higher values of the appearance energies and a more complex shape of the curves in the near-threshold region, which is indicative of the fact that in some cases (e.g., for the production of $C_2H_4^+$), several processes contribute to the formation of these fast ions. In the case of CH_3^+, we find (see Fig. 5), for CH_3^+ ions with a kinetic energy of ~3 eV (peak maximum in Fig. 1), one major onset at ~29 eV. This major onset is consistent with the value of 30.8 eV reported by Olmsted et al. [19] and with the value of (30.6±0.5) eV reported by Ehrhardt and Tekaat [14] for ions with a kinetic energy of 3.4 eV and falls nicely on the calculated line in their Fig. 6, relating the measured appearance energy with the kinetic energy. According to these authors, extrapolation of this line yields a value for the appearance energy without kinetic energy release of ~25 eV. This onset corresponds most likely to the break-up of the doubly charged $C_3H_8^{++}$ ion that is formed initially in the collision of the incident electron with the neutral C_3H_8 molecule

$$C_3H_8^{2+} \rightarrow CH_3^+ + H_2 + C_2H_3^+. \quad (3)$$

This process has a thermochemical minimum energy of ~24.5 eV [14], which agrees nicely with the extrapolated value of 25 eV. It is interesting to note that Ehrhardt and Tekaat also report appearance energies for CH_3^+ ions with kinetic energies <2 eV yielding extrapolated appearance energies of 22 and 20 eV [14]. As already mentioned above, we do not see such ions, which is most likely because of the higher energy resolution in our experiment.

In the case of $C_2H_4^+$, we find at the peak maximum of the fast fragment component (i.e., at ~1.3 eV in Fig. 2) a major onset at ~31 eV, which is consistent with the value of 31.6 eV reported earlier [14] for a kinetic energy of 1.55 eV. The extrapolated value of [14] with a value of 27.2 eV is consistent with the thermochemical minimum of 26.5 eV for reaction (4):

$$C_3H_8^{2+} \rightarrow C_2H_4^+ + H_2 + CH_2^+. \quad (4)$$

We also see a long, extended tail down to ~20 eV, which Ehrhardt and Tekaat [14] attributed to a parasitic contribution from the quasi-thermal ions in their signal. As our measurement separates the fast ions from the quasi-thermal ions, we must conclude that this tail is also attributable to processes leading to the formation of fast $C_2H_4^+$ fragment ions. Possible processes other than reaction (4) also leading to fast $C_2H_4^+$ ions include

$$C_3H_8^{++} \rightarrow C_2H_4^+ + CH_4^+. \quad (5)$$

In accordance with the experimental results, the thermochemical minimum energy for reaction (5) is ~2.5 eV lower than that of reaction (4). Thus, it is apparent from our high-resolution measurements that several processes contribute to the formation of the fast $C_2H_4^+$ fragment ions in contrast to what was concluded from previous studies.

4. Summary

Measurements of the kinetic energy distributions of fragment ions produced by electron-impact dissociative ionization of propane were carried out using a two-sector-field mass spectrometer in conjunction with the retarding field method. This technique achieves a higher energy resolution, albeit at much reduced ion signals and at a significant loss of energetic fragment ions compared to the conventional ion deflection technique, which has been used extensively by other groups in the past. The higher energy resolution used in the present experiments results in a complete separation of the thermal and quasi-thermal fragment ions from the energetic fragment ions. This, in turn, reveals that the energetic fragment ions have a much narrower kinetic energy distribution than previously assumed. Because of the comparatively weak ion signals, further studies such as separate appearance energy determinations for, respectively, the slow and fast fragment ions could only be carried out for the CH_3^+ and $C_2H_4^+$ fragment ions. Our appearance energy measurements for the fast $C_2H_4^+$ fragment ions show conclusively that several processes contribute to the formation of these energetic ions.

Acknowledgments

This work has been partially carried out within the Association EURATOM-ÖAW and supported by the FWF, Wien, and in part by a grant from the U.S. National Aeronautics and Space Administration (NASA) under grant NAG5-8971.

References

[1] L.G. Christophorou (Ed.), Electron Molecule Interactions and their Applications, Academic Press, Orlando, FL, 1984.
[2] T.D. Märk, G.H. Dunn (Eds.), Electron Impact Ionization, Springer, Wien, 1985.
[3] L.C. Pitchford, B.V. McKoy, A. Chutjian, S. Trajmar (Eds.), Swarm Studies and Inelastic Electron-Molecule Collisions, Springer, New York, 1987.
[4] L.H. Toburen, Y. Hatano, Z. Herman, T.D. Märk, S. Trajmar, J.J. Smith, IAEA-TECDOC 506 (1989) 23.
[5] R.K. Janev, H.W. Drawin (Eds.), Atomic and Plasma-Material Interaction Processes on Controlled Thermonuclear Fusion, Elsevier, Amsterdam, 1993.
[6] R.K. Janev (Ed.), Atomic and Molecular Processes in Fusion Edge Plasmas, Plenum, New York, 1995.
[7] W.O. Hofer, J.Roth, (Eds.), Physical Processes of the Interaction of Fusion Plasmas with Solids, Academic Press, San Diego, 1996.
[8] J.P. Mohr, W.L. Wiese, (Eds.), Atomic and Molecular Data and their Applications, AIP Conference Proceedings 434, AIP, Woodbury, NY, 1998.
[9] H.U. Poll, V. Grill, S. Matt, N. Abramzon, K. Becker, P. Scheier, T.D. Märk, Int. J. Mass Spectrom. Ion Processes 177 (1998) 143.
[10] J.W. Au, G. Coppe, C.E. Brion, Chem. Phys. 173 (1993) 241.
[11] B.L. Schram, M.J. van der Wiel, F.J. de Heer, H.R. Moustafa, J. Chem. Phys. 44 (1966) 49.
[12] N. Djuric, I. Cadez, M. Kurepa, Int. J. Mass Spectrom. Ion Processes 108 (1991) R1.
[13] V. Grill, G. Walder, D. Margreiter, T. Rauth, H.U. Poll, P. Scheier, T.D. Märk, Z. Phys. D 25 (1993) 217.
[14] H. Ehrhardt, T. Tekaat, Z. Naturforschg. 19a (1964) 1382.
[15] R. Taubert, Z. Naturforschg. 19a (1964) 484.
[16] R. Fuchs, R. Taubert, Z. Naturforschg. 19a (1964) 494.
[17] R. Taubert, Z. Naturforschg. 19a (1964) 911.
[18] R. Fuchs, R. Taubert, Z. Naturforschg. 19a (1964) 1181.
[19] J. Olmsted III, K. Street, Jr., A.S. Newton, J. Chem. Phys. 40 (1964) 2114.
[20] D.K. Sen Sharma, J.L. Franklin, Int. J. Mass Spectrom. Ion Phys. 13 (1974) 139.
[21] A.I. Ossinger, E.R. Weiner, J. Chem. Phys. 65 (1976) 2892.
[22] H.U. Poll, C. Winkler, D. Margreiter, V. Grill, T.D. Märk, Int. J. Mass Spectrom. Ion Processes 112 (1992) 1.
[23] C. Lifshitz, M. Shapiro, J. Chem. Phys. 46 (1967) 4912.
[24] R. Stockbauer, M.G. Inghram, J. Chem. Phys. 54 (1971) 2242; R. Stockbauer, M.G. Inghram, J. Chem. Phys. 65 (1976) 4081.
[25] P. Wolkoff, J.L. Holmes, J. Am. Chem. Soc. 100 (1978) 7346.
[26] K.F. Donchi, R.T. Brownlee, P.J. Derrick, Chem. Soc. Chem. Commun. (1980) 1061.
[27] J.P. Gilman, T. Hsieh, G.G. Meisels, J. Chem. Phys. 76 (1982) 3497.
[28] M. Medved, R.G. Cooks, J.H. Beynon, Int. J. Mass Spectrom. Ion Processes 19 (1976) 179.
[29] J.L. Holmes, A.D. Osborne, Org. Mass Spectrom. 13 (1978) 133.
[30] S. Matt, O. Echt, A. Stamatovic, T.D. Märk, J. Chem. Phys. 113 (2000) 616.
[31] S. Olivella, A. Sole, D.J. McAdoo, J. Am. Chem. Soc. 118 (1996) 9368.
[32] H.M. Rosenstock, K. Draxl, B.W. Steiner, J.T. Herron, J. Phys. Chem. Ref. Data 6 (1977) L1.
[33] R.E. Fox, J.A. Hipple, Rev. Sci. Instrum. 19 (1948) 462.
[34] J.A. Hipple, J. Phys. Colloid. Chem. 52 (1948) 456.
[35] H.D. Hagstrum, Revs. Mod. Phys. 23 (1951) 185.
[36] R.J. Kandel, Phys. Rev. 91 (1951) 436.
[37] R.J. Kandel, J. Chem. Phys. 22 (1954) 1496.
[38] N. Kouchi, M. Ohno, K. Ito, N. Oda, Y. Hatano, Chem. Phys. 67 (1982) 287.
[39] M. Darrach, J.W. McConkey, J. Chem. Phys. 95 (1991) 754.
[40] J.C. Syage, J. Chem. Phys. 97 (1992) 6085.
[41] C. Tian, C.R. Vidal, J. Chem. Phys. 108 (1998) 927.
[42] S. Wei, W.B. Tzeng, A.W. Castleman Jr., J. Chem. Phys. 92 (1990) 332.
[43] I. Torres, R. Martinez, M.N. Sanchez Rayo, F. Castano, Chem. Phys. Lett. 328 (2000) 135.
[44] R.P. Tuckett, E. Castellucci, M. Bonneau, G. Dujardin, S. Leach, Chem. Phys. 92 (1985) 43.
[45] I. Powis, P.I. Mansell, C.J. Danby, Int. J. Mass Spectrom. Ion Phys. 32 (1979) 15.
[46] I. Powis, Chem. Phys. 68 (1982) 251.
[47] K. Johnson, I. Powis, C.J. Danby, Chem. Phys. 70 (1982) 329.
[48] I. Powis, J. Chem. Phys. 99 (1993) 3436.
[49] P.A. Hatherly, D.M. Smith, R.P. Tuckett, Z. Phys. Chemie 195 (1996) 97.
[50] G. Jarvis, D.P. Seccombe, R.P. Tuckett, Chem. Phys. Lett. 315 (1999) 287.
[51] G. Jarvis, C.A. Mayhew, R.Y.L. Chim, R.A. Kennedy, R.P. Tuckett, Chem. Phys. Lett. 320 (2000) 104.
[52] P.W. Zetner, M. Darrach, P. Hammond, W.B. Westerveld, R.L. McConkey, J.W. McConkey, Chem. Phys. 124 (1988) 453.
[53] T. Ogawa, T. Tomura, K. Nakashima, H. Kawazumi, J. Chem. Phys. 88 (1988) 4263.
[54] C. Mair, T. Fiegele, F. Biasioli, R. Wörgötter, V. Grill, M. Lezius, T.D. Märk, Plasma Sources Sci. Technol. 8 (1999) 191.
[55] T. Fiegele, Diploma Thesis, Universität Innsbruck (1998), unpublished.
[56] F.L. Mohler, V.H. Dibeler, R.M. Reese, J. Chem. Phys. 22 (1953) 394.
[57] H.E. Stanton, J. Chem. Phys. 30 (1959) 1116.
[58] T. Tsuchiya, J. Chem. Phys. 36 (1962) 568.
[59] T. Fiegele, G. Hanel, I. Torres, M. Lezius, T.D. Märk, J. Phys. B33 33 (2000) 4263.
[60] J. Appell, J. Durup, F. Heitz, Adv. Mass Spectrom. 3 (1966) 457.
[61] W.G. Mallard, P.J. Linstrom, 2000 NIST Standard Reference Database E, Vol. 69, Gaithersburg, MD, National Institute of Standards and Technology. Available at: http://webbook.nist.gov.